Oxygen Evolution Reaction

International Edition: DOI: 10.1002/anie.201505320
German Edition: DOI: 10.1002/ange.201505320

Ultrathin Co_3S_4 Nanosheets that Synergistically Engineer Spin States and Exposed Polyhedra that Promote Water Oxidation under Neutral Conditions

Youwen Liu, Chong Xiao, Mengjie Lyu, Yue Lin, Weizheng Cai, Pengcheng Huang, Wei Tong, Youming Zou, and Yi Xie**

Abstract: *Development of efficient and affordable electrocatalysts in neutral solutions is paramount importance for the renewable energy. Herein, we report that the oxygen evolution reaction (OER) performance of Co_3S_4 under neutral conditions can be enhanced by exposed octahedral planes and self-adapted spin states in atomically thin nanosheets. A HAADF image clearly confirmed that the active octahedra with Jahn–Teller distortions were exposed exclusively. Most importantly, in the atomically thin nanosheets, the spin states of Co^{3+} in the octahedral self-adapt from low-spin to high-spin states. As a result, the synergistic effect endow the Co_3S_4 nanosheets with superior OER performance, with exceptional low onset overpotentials of circa 0.31 V in neutral solutions, which is state-of-the-art among inorganic non-noble metal compounds.*

The growing global energy crisis and environmental contamination compel us to spare no effort into the rational exploration of highly efficient and affordable catalysts for clean and sustainable energy generation, especially for the oxygen evolution reaction (OER), which in particular is a pivotal process for many renewable energy options.[1–3] Owing to their diversity, intrinsic activities, and abundance, spinel compounds provide promising alternatives for OER electrocatalysts to break through the limitation of having to use precious metals.[4–6] However, contemporarily spinel electrocatalysts are predominately operated in strong alkaline solutions, which significantly hinders their industrial applications. Moreover, the catalytic ability of spinel electrocatalysts is a serious limit in a neutral pH environment. Under these circumstances, the exploitation of the superior activity spinel catalysts under neutral conditions is deemed to be particularly critical for sustainable energy conversion.

The spinel structures contain trivalent B ions in the octahedral sites and divalent A ions in the tetrahedral sites.[7] However, the octahedral sites are catalytic active, whereas the tetrahedral sites are almost inert.[8] Therefore, constructing a spinel surface with predominantly exposed octahedral planes is highly desirable for the acquisition of highly active spinel OER catalysts. Following Ratnasamy, we can differentiate several low-index surface planes in spinels (Figure 1 a). The F{111} plane solely exposes octahedral coordinated cations, suggesting that these facets should possess the highest reactivity compared to other crystal facets.[9] Consequently, to optimize active sites for developing efficient OER activity, the design of spinels with exclusive exposure of F{111} planes may be of vital significance. On the other hand, the spin states, which determine the occupancy of e_g orbital governing many pivotal reaction steps, is also a key factor for OER.[3,10–12] This fact implies that modulation of electronic configuration may also be a general and effective strategy for the improvement of OER reactivity under neutral conditions in diversity spinel compounds.

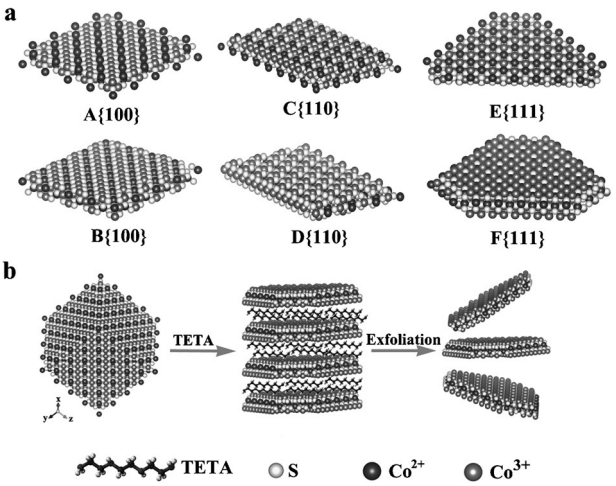

Figure 1. Diagrams of low-index surface planes and representation of the fabrication process for Co_3S_4 atomically thin nanosheets (CSATN). a) Six different low-index surface planes. b) The strategy for manufacturing CSATN from lamellar Co_3S_4/TETA hybrid precursors.

The two key issues mentioned above suggest that modulation of spin states in uniquely exposed active planes should be an effective strategy for the significant promotion of OER performance. Fortunately, the emerged ultrathin nanosheets provide us a faultless platform to achieve this goal. First, the 2D configuration could offer solely exposure of

[*] Y. W. Liu, Dr. C. Xiao, M.-J. Lyu, Dr. Y. Lin, W. Z. Cai, P. C. Huang, Prof. Y. Xie
Hefei National Laboratory for Physical Sciences at the Microscale
Collaborative Innovation Center of Chemistry for Energy Materials
University of Science and Technology of China
Hefei, Anhui, 230026 (P.R. China)
E-mail: cxiao@ustc.edu.cn
yxie@ustc.edu.cn
Prof. W. Tong, Prof. Y. M. Zou
High Magnetic Field Laboratory, Chinese Academy of Sciences
Hefei, Anhui, 230031 (P.R. China)

Supporting information for this article is available on the WWW under http://dx.doi.org/10.1002/anie.201505320.

specific crystal planes with active sites. Moreover, atomically nanosheets are accustomed to generate structural disorder, which usually company with electronic configuration change.[13] Based on the above considerations, the synergistic manipulation of exposed octahedral planes and the electronic configuration of spinel compounds in atomic-level nanosheets would be an extremely efficient strategy to pursue efficient electrocatalysts under the neutral solutions. Co_3S_4, as a conventional spinel, would be a competitive candidate for utilization in water oxidation owing to its attractive metallic nature (Supporting Information, Figure S1), which could ensure fast charge migration during the electrocatalytic pathway. Herein, we propose the controllable synthesis of CSATN with drastically enhanced OER performance under neutral conditions through the synergistic effect of exclusively exposed octahedral planes and self-adapted spin states.

The non-layer-structured CSATN were rationally manufactured by ultrasound exfoliation treatment from an intermediate Co_3S_4/TETA (TETA = triethylenetetramine) hybrid precursor (Supporting Information, Figure S2). To explore the structural information of the nanosheet, Raman spectroscopy was first carried out. As shown in Figure 2a, the corresponding Raman peaks of CSATN could be indexed to the spinel Co_3S_4. Their Raman modes reveal obvious broadening and weakening compared with that of bulk counterpart (Supporting Information, Figure S3), which is mainly ascribed to surface structural distortion of CSATN. Furthermore, the TEM image of the products (Figure 2b) exhibits a freestanding sheetlike morphology with the transparency character revealing the ultrathin configuration, which is further shown by the AFM image in Figure 2c. The AFM image and corresponding height profile displayed the sheetlike morphology with an average thickness of approximately 1.0 nm, which is consistent with the thickness of [CoS] slab in the intermediate Co_3S_4/TETA hybrid (Supporting Information, Figure S2). To illuminate the exposed plane of CSATN, the XRD pattern of a layer-by-layer assembled film for exfoliated products clearly displays the sole diffraction peak assigned to the (111) facet of cubic Co_3S_4, which provides an undoubtedly evidence for the CSATN along the [111] direction. Moreover, HRTEM image and the hexagonal-shaped SAED well agree with nanosheets along [111] orientation. The conclusion that CSATN preferential exposed the (111) facet can be drawn with a certain degree of confidence from the above the XRD and HRTEM characterization. For direct visualization to confirm active planes with solely exposed octahedral coordinated cations, high-angle annular dark field (HAADF) imaging could be carried out (Figure 3c).

Notably, pioneering experimental results have revealed that spin states of active atoms is significant factors in enhancing catalytic activity, which is highly related to oxygen surface exchange and metal coordination atom bond strength.[14] Bearing this in mind, the electronic configuration

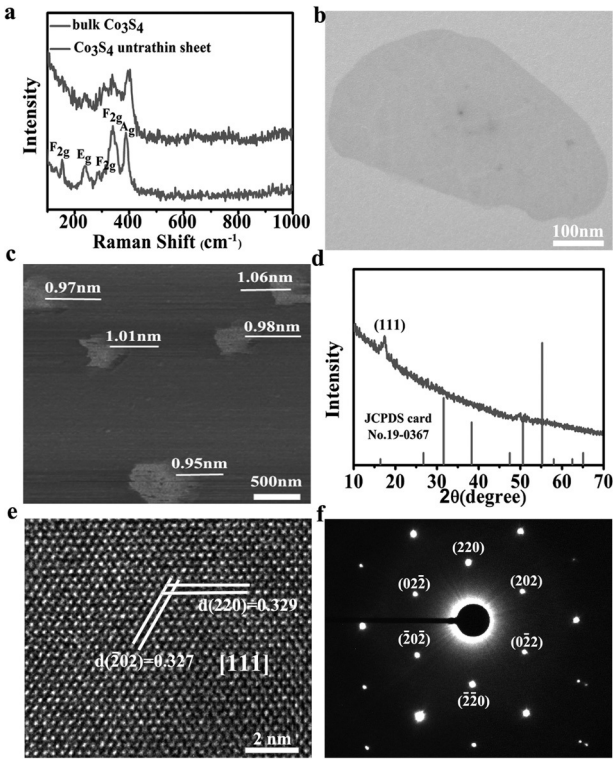

Figure 2. Microstructural characterization. a) Raman spectra. b) TEM image. c) Atomic force microscopy image (AFM). d) XRD pattern for a Co_3S_4 ATN SLB film fabricated by LBL assembly. e,f) HRTEM and SAED analysis.

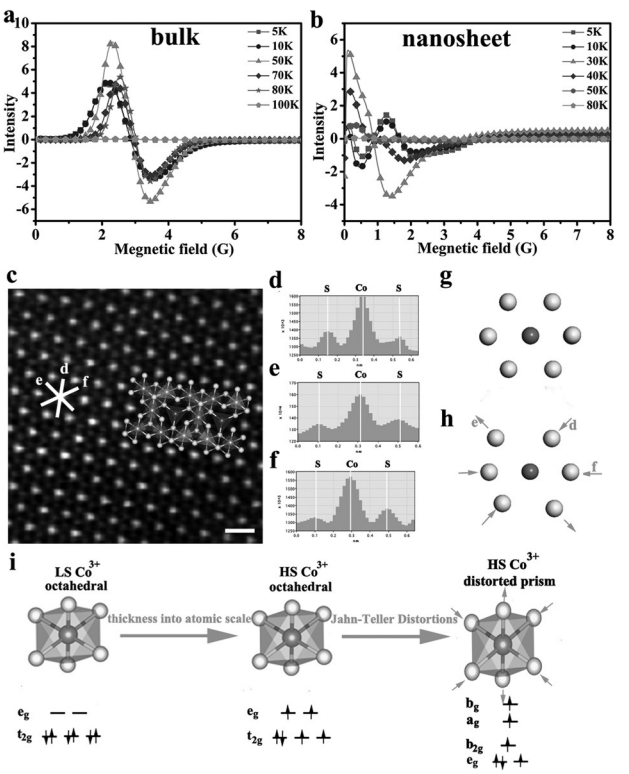

Figure 3. Visualization of high-spin-state-induced Jahn–Teller distortion of CSATN. a,b) Temperature-dependent EPR of bulk and CSATN. c) HAADF images of CSATN. Scale bars: 0.5 nm. d–f) HAADF intensity line profiles along the directions signed by the white lines in (c). g,h) [111] zone axis section view of original octahedral and Jahn–Teller distortion (the specific distances are shown in the Supporting Information, Figure S4 and Table S1). i) Representations of structural transformation by reducing its thickness to the atomic scale.

of the Co cation in octahedral coordination could be revealed by the temperature-dependent electron paramagnetic resonance (EPR), which is a powerful technique to detect the 3d electron configuration (both e_g and t_{2g} electrons) of transition metals.[15] We take the electronic structure of the cobalt ions at the octahedral into account because tetrahedral sites in spinel structure are inert. The Figure 3a clearly shows single LS Co^{2+} signal without Co^{3+} signal in bulk Co_3S_4, which confirms d^6 electron configurations of Co^{3+} in the form of $t_{2g}^6e_g^0$. In stark contrast, the EPR spectrum of CSATN reveals significant differences relative to bulk Co_3S_4, as shown in Figure 3b. The absence of the uncoupled Co^{2+} signal including the low-spin and high-spin states near 3.5 G over those whole temperature range suggests the Co^{2+} ferromagnetic coupled with surrounding other Co ions. Moreover, the phenomenon of a shifting of the spectral weight to lower magnetic fields at low temperatures in Figure 3b further infers the existence of ferromagnetic coupling in CSATN, which concludes all of Co ion with a high-spin state. In other words, the Co^{3+} in CSATN manifests a high-spin state. Previous reports have shown that as-exfoliated sheets undergo strain,[16] which could induce a change in the Co spin state from low spin to high spin.[14] In this regard, tuning the spin state by reducing thickness into the atomic scale may be attributed to the above possible reasons. What is noteworthy is that HS Co^{3+} in octahedral ($t_{2g}^4e_g^2$) will distort (Jahn–Teller effect) to remove the degeneracy and form a lower energy (and by consequence, lower symmetry) system, because it possesses a degenerate electronic ground state (Supporting Information, Table S2).[17] As a consequence, the octahedral complex will either elongate or compress the *z* ligand bonds. To visualize the Jahn–Teller distortion of HS Co^{3+} in CSATN at an atomic scale, the HAADF imaging method, which has already proved to be a powerful technology for direct visualization the atoms, defects, and edges in 2D crystals, was performed.[18,19] In this regard, the HAADF image of CSATN is displayed in Figure 3c. It is seen that brighter and less bright spots with periodically arrangement are clearly resolved in the HAADF images, which correspond to the two distinct atoms, namely Co and S. The inset in Figure 3c shows the corresponding F(111) plane with sole exposed octahedra coordinated to help visualize surface atomic arrangements. The overall structure matches that of F (111) facets of Co_3S_4, for the notation of the planes solely expose octahedral coordinated cations. Despite all this, the feature of slight lattice mismatch between the standard lattice and the HAADF atoms arrangement deriving from the Jahn–Teller distortion is worth noting. Furthermore, the Co atoms and S atoms are distinctly confirmed in the HAADF images in Figure 3c. HAADF line intensity profiles along the directions signed by the lines in Figure 3c are shown in Figure 3d–f. The models of Co and S atoms exhibit the relative atomic column pattern through alternating peak positions, corresponding to the embedded simulative model in Figure 3c. From the peak position, we observe six distinct Co–S distances (Supporting Information, Table S1), which are substantially different from the pristine Co_3S_4 lattice. We reasonably used HAADF imaging to help visualize and demonstrate that elongation of Jahn–Teller distortions occur, as displayed in Figure 3g and h. From the above analysis, we propose and illustrate the most likely structural transformation resulting from reducing its thickness into atomic scale in Figure 3i. Briefly, strained exfoliated CSATN induces changes in the Co spin states, and the consequent HS Co^{3+} in octahedra ($t_{2g}^4e_g^2$) will distort (Jahn–Teller effect) to remove the degeneracy and form a slightly distorted prism.

More importantly, as reported previously, local lattice distortions seem to facilitate the high OER activity. For instance, the Manthiram group reported that the OER activity of $LiCoO_2$ increases with increasing firing temperature, as a result of which surface strains arising from a slight lattice mismatch between the LT-$LiCoO_2$ and HT-$LiCoO_2$.[5] The Shao-Horn group also reported that the large activity of $Sr_4Mn_2CoO_9$ can be attributed to HS Co^{2+} in distorted prisms.[20] Moreover, Suib et al. investigated all manganese oxides, and found that the electrocatalytic performance averagely promotes when Mn–O bonds are distorted in the structure.[21] Certain conclusions can be drawn from these studies, and the local lattice distortions play a pivotal role in maximizing the OER activity, which could provide new guidelines for develop in highly active electrocatalysts.

To confirm the conjecture, the electrocatalytic activity in phosphate buffer solution is evaluated. Figure 4a shows linear sweep voltammetry polarization curves of all the samples. The constructed catalyst exhibited an exceptionally small onset overpotential (η) of 0.31 V for catalytic O_2 evolution, representing the state-of-the-art for OER catalysts under neutral conditions involving inorganic non-noble metal compounds (Supporting Information, Tables S3 and S4). In stark contrast, the onset overpotentials of bulk Co_3S_4 and Co_3S_4/TETA were strictly required (690 mV and 580 mV, respectively), which only manifests inferior OER activity. Meanwhile, it is worth noting that the current densities of CSATN were 3.97 mA cm^{-2} at modest overpotential 0.7 V, revealing approximately 24 times than bulk counterpart. It can be summarized that negative overpotential and large current density indicate that CSATN is an outstanding active OER catalyst at the neutral pH. A vital metric for viability of an OER catalyst is Tafel slope which could allow the evaluation of the OER increment rate. The resulting Tafel slope of CSATN is as low as 151 mV dec^{-1} (Figure 4b), whereas bulk Co_3S_4 and Co_3S_4/TETA possess much higher Tafel slopes of 192 mV dec^{-1} and 235 mV dec^{-1}. The small Tafel slope of the CSATN is advantageous for practical utilizations owing to it will contribute to an intensely increment of OER rate with applied overpotential. Furthermore, the TOFs in Figure 4c were calculated and estimated based on the assumption that all the Co ions in octahedral coordination present in the material were catalytically active. Of note, the TOFs of CSATN were 0.00605 s^{-1} (Supporting Information, Table S3) at an overpotential of 0.7 V, affording much greater TOFs than either bulk counterpart or Co_3S_4/TETA. Besides high OER activity, Figure 4d depicts a CSATN catalyst that exhibits superior durability in neutral solutions. After 5000 potential cycles in aqueous phosphate buffer solution, the CSATN almost appeared analogous *j*–*V* curves as initial electrocatalyst, with insignificant attenuation of the current density. In other words, the CSATN has the excellent stability

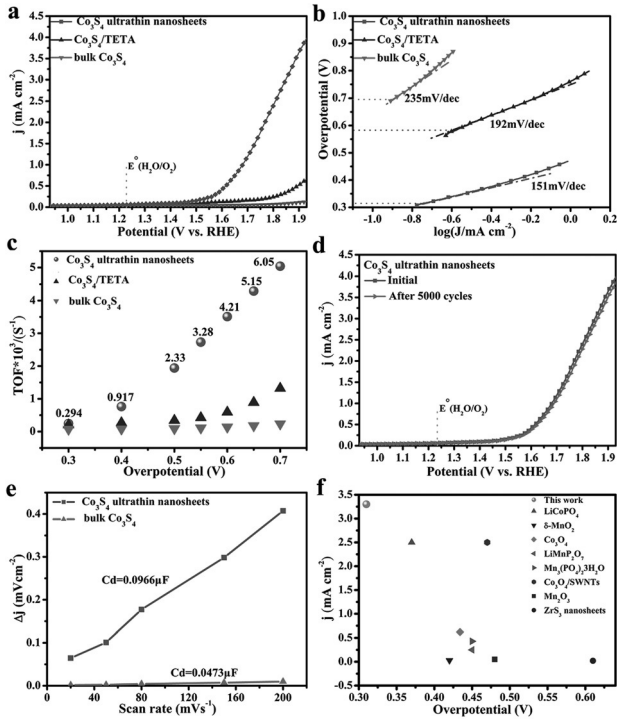

Figure 4. Water oxidation performance in neutral solution. a) LSV polarization curves and b) corresponding Tafel plots. c) A plot of TOFs with respect to Co atoms at different overpotentials. d) Stability test. e) The differences in current density variation plotted against scan rate fitted to a linear regression enables the estimation of C_d. f) The onset overpotential and current densities (at an overpotential of 0.65 mV) of some inorganic water oxidation electrocatalysts in neutral solution (the specific values and relevant references are given in the Supporting Information, Table S4 and the corresponding references).

to withstand accelerated degradation under the long term electrochemical cycling process. Further, the excellent chemical stability of the CSATN was demonstrated (Supporting Information, Figure S5), implying that only faint degradation of OER performance at neutral pH occurs after six months of storage under ambient conditions. In combination with an omnibearing electrochemical test, we can unambiguously conclude that the CSATN is a novel electrocatalyst material with exceptional OER activity in a neutral environment, which hold great significance for actually applications. Furthermore, the water oxidation activity of CSATN under the strongly alkaline conditions was also investigated. The comprehensively electrochemical measurements are shown in the Supporting Information, Figure S6. The CSATN manifest an OER onset overpotential as low as 0.28 V, small Tafel slopes of 48 mV dec^{-1}, and large turnover frequencies of 0.17 s^{-1}, which the integrated performance outperforms most of pure spinel OER electrocatalysts (Supporting Information, Figure S6, Tables S5 and S6).

To test CSATN with a high exposure of effective active sites, electrochemical double layer capacitances (C_d) are measured, which is expected to be linearly proportional to the effective surface area.[22] As shown in Figure 4e, the CSATN exhibits much larger C_d of 0.0966 μF, which is more than roughly 20 times more than the bulk counterpart in a neutral environment. Furthermore, the ultimate confirmation could be attained in strongly alkaline solution (Supporting Information, Figures S6 and S7). Based on the electrochemical test, the viability of our constructed catalyst with high exposure of effective active sites has been further confirmed. Therefore, the dramatically enhanced OER activity both neutral and alkaline environment of CSATN with simultaneous optimization active sites and fabrication distorted structure can be attributed to the following aspects: 1) The (111) facet of Co_3S_4 only exposes the highest reactivity octahedral coordinated cations and the optimum surface atomic arrangements favorable for water oxidation; 2) strained exfoliated nanosheets induce changes in spin state and subsequently HS Co^{3+} undergo Jahn–Teller distortion; the local lattice distortions may play a role in maximizing the OER.

In summary, we have presented a scalable strategy to synergistically engineer spin states and exposed polyhedra in ultrathin nanosheets for development of high-activity water oxidation electrocatalysts in both a neutral and alkaline environment. First, we successfully constructed CSATN with exclusively Jahn–Teller-distorted octahedra exposed, which is clearly confirmed by a HAADF image. Even more importantly, the spin states of Co^{3+} in the exposed octahedral self-adapted from low-spin to high-spin states as the nanosheet configurations thinned to be atomically thick. Benefiting from the synergistic effect of the atom structural and electronic configuration modulations, these CSATN manifest an OER onset overpotential as low as 0.31 V and superlarge polarization current of about 3.97 mA cm^{-2} at an overpotential of 0.7 V at neutral pH, the integrated performance holds the state-of-the-art record among the inorganic non-noble metal compounds. As a consequence, the impressive water oxidation performance of the catalyst can be anticipated to be a fresh candidate to replace noble metals. Furthermore, the success of simultaneous optimization exposed octahedral active planes and self-adapted spin states by innovative establishing atomically thin nanosheets featured in this work undoubtedly provide profound perspectives in pursuing efficient electrocatalysts.

Acknowledgements

We thank Dr. J. H. Su (Hefei National Laboratory for Physical Sciences at the Microscale and Department of Modern Physics, University of Science and Technology of China) for the helpful discussion of the interpreted EPR spectra. This work was financially supported by National Basic Research Program of China (2015CB932302), National Natural Science Foundation of China (21401182, 21331005, 11321503) and 91422303), China Postdoctoral Science Foundation (No. 2014M550347), Key Laboratory of Neutron Physics (CAEP 2014DB02), the Fundamental Research Funds for the Central University (WK2340000063 and WK 2060190027), and the Opening Project of the Jiangsu Key Laboratory for Environment Functional Materials (No. SJHG1301).

Keywords: cobalt · exposed polyhedra · nanosheets · spin states · water oxidation

How to cite: *Angew. Chem. Int. Ed.* **2015**, *54*, 11231–11235
Angew. Chem. **2015**, *127*, 11383–11387

[1] H. B. Gray, *Nat. Chem.* **2010**, *2*, 7.
[2] M. W. Kanan, D. G. Nocera, *Science* **2008**, *321*, 1072–1075.
[3] J. Suntivich, K. J. May, H. A. Gasteiger, J. B. Goodenough, Y. Shao-Horn, *Science* **2011**, *334*, 1383.
[4] F. Y. Cheng, J. Shen, B. Peng, Y. D. Pan, Z. J. Tao, J. Chen, *Nat. Chem.* **2011**, *3*, 79–84.
[5] T. Maiyalagan, K. A. Jarvis, S. Therese, P. J. Ferreira, A. Manthiram, *Nat. Commun.* **2014**, *5*, 3949.
[6] J. Bao, X. D. Zhang, B. Fan, J. J. Zhang, M. Zhou, W. L. Yang, X. Hu, H. Wang, Y. Xie, *Angew. Chem. Int. Ed.* **2015**, *54*, 7399–7404; *Angew. Chem.* **2015**, *127*, 7507–7512.
[7] W. H. Bragg, *Nature* **1915**, *95*, 561.
[8] J. P. Jacobs, A. Maltha, J. G. Reintjes, J. Drimal, V. Ponec, H. H. Brongersma, *J. Catal.* **1994**, *147*, 294–300.
[9] H. Knözinger, P. Ratnasamy, *Catal. Rev. Sci. Eng.* **1978**, *17*, 31–71.
[10] A. Grimaud, K. J. May, C. E. Carlton, Y. L. Lee, M. Risch, W. T. Hong, J. Zhou, Y. Shao-Horn, *Nat. Commun.* **2013**, *4*, 2439.
[11] Y. W. Liu, H. Cheng, M. J. Lyu, S. J. Fan, Q. H. Liu, W. S. Zhang, Y. D. Zhi, C. M. Wang, C. Xiao, S. Q. Wei, B. J. Ye, Y. Xie, *J. Am. Chem. Soc.* **2014**, *136*, 15670–15675.
[12] J. H. Huang, J. T. Chen, T. Yao, J. F. He, S. Jiang, Z. H. Sun, Q. H. Liu, W. R. Cheng, F. C. Hu, Y. Jiang, Z. Y. Pan, S. Q. Wei, *Angew. Chem. Int. Ed.* **2015**, *54*, 8722–8727; *Angew. Chem.* **2015**, *127*, 8846–8851.
[13] Y. F. Sun, H. Cheng, S. Gao, Z. H. Sun, Q. H. Liu, F. C. Lei, T. Yao, J. F. He, S. Q. Wei, Y. Xie, *Angew. Chem. Int. Ed.* **2012**, *51*, 8727–8731; *Angew. Chem.* **2012**, *124*, 8857–8861.
[14] W. T. Hong, M. Gadre, Y. L. Lee, M. D. Biegalski, H. M. Christen, D. Morgan, Y. Shao-Horn, *J. Phys. Chem. Lett.* **2013**, *4*, 2493–2499.
[15] J. J. Scepaniak, C. S. Vogel, M. M. Khusniyarov, F. W. Heinemann, K. Meyer, J. M. Smith, *Science* **2011**, *331*, 1049–1052.
[16] D. Voiry, H. Yamaguchi, J. Li, R. Silva, D. C. Alves, T. Fujita, M. Chen, T. Asefs, V. B. Shenoy, G. Eda, M. Chhowalla, *Nat. Mater.* **2013**, *12*, 850–855.
[17] R. Englman, *The Jahn–Teller effect in molecules and crystals*, New York, Wiley-Interscience, **1972**.
[18] Z. Liu, K. Suenaga, Z. Wang, Z. Shi, E. Okunishi, S. Iijima, *Nat. Commun.* **2011**, *2*, 213.
[19] X. Li, X. Ma, D. Su, L. Liu, R. Chisnell, S. P. Ong, H. Chen, A. Toumar, J.-C. Idrobo, Y. Lei, J. Bai, F. Wang, J. W. Lynn, Y. S. Lee, G. Ceder, *Nat. Mater.* **2013**, *12*, 586–592.
[20] A. Grimaud, C. E. Carlton, M. Risch, W. T. Hong, K. J. May, Y. Shao-Horn, *J. Phys. Chem. C* **2013**, *117*, 25926–25932.
[21] Y. Meng, W. Song, H. Huang, Z. Ren, S. Y. Chen, S. L. Suib, *J. Am. Chem. Soc.* **2014**, *136*, 11452–11464.
[22] J. F. Xie, J. J. Zhang, S. Li, F. Grote, X. D. Zhang, H. Zhang, R. X. Wang, B. C. Pan, Y. Xie, *J. Am. Chem. Soc.* **2013**, *135*, 17881–17888.

Received: June 11, 2015
Published online: July 31, 2015

